Materials Characterization, Volume 161, March 2020, Article number 110167
DOI: 10.1016/j.matchar.2020.110167

A new method for assessing the utility of Powder Bed Fusion (PBF) feedstock through life

Nima E. Gorji[1,*], Prateek Saxena[2], Martin Corfield[3], Adam Clare[3], Jean-Pascal Rueff[4,5,6], Justin Bogan[7], Pierre. G. M. González[4,7], Matthew Snelgrove[7], Greg Hughes[7,8], Robert O'Connor[6], Ramesh Raghavendra[9], Dermot Brabazon[1]

[1]I-Form Additive Manufacturing Research Centre, Dublin City University, Dublin 9, Ireland
[2] Sustainable Manufacturing Systems Centre, School of Aerospace, Transport and Manufacturing, Cranfield University, Bedfordshire, UK
[3] School of Advanced Manufacturing, University of Nottingham, Nottingham, UK
[4]Institute of Engineering and Technology, Autonomous University of Ciudad Juarez, Juarez, Mexico
[5]Synchrotron SOLEIL L'Orme des Merisiers, Saint-Aubin, Essonne, France.
[6]Sorbonne Université, CNRS, Laboratoire de Chimie Physique- Matiére et Rayonnement, LCPMR, Paris, France.
[7]School of Physical Sciences, Dublin City University, Glasnevin, Dublin 9, Ireland.
[8]National Centre for Plasma Science and Technology, Dublin City University, Glasnevin, Dublin 9, Ireland.
[9]SEAM Research Centre, Waterford Institute of Technology, Waterford, Ireland.
*Corresponding Author: Email: nima.gorji@i-form.ie; nima.gorji@dcu.ie; Tel: +35317007696

ABSTRACT

Recycling metallic powders used in the additive manufacturing (AM) process is essential for reducing the process cost, manufacturing time, energy consumption, and metallic waste. In this paper, the focus is on pore formation in recycled powder particles of stainless steel 316L during the selective laser melting process. We have introduced the concept of optimizing the powder bed's printing area in order to see the extent of the affected powders during the 3D-printing process. X-ray Computed Tomography (XCT) is used to characterize the pores inside the particles. The results from image processing of the tomography (rendered in 3D format) indicate a broader pore size distribution and a higher pore density in recycled powders compared to their virgin counterparts. To elucidate on this, the Electron Dispersion spectroscopy (EDX) analysis and Synchrotron-based Hard X-ray Photoelectron Spectroscopy (HAXPES) were performed to reveal the chemical composition distribution across the pore area and bulk of the recycled powder particles. Higher concentrations of Fe, Cr, and Ni were recorded on the interior wall of the pore in recycled particles and higher Mn, S and Si concentrations were recorded in the outer layer around the pore area and on the surface of the recycled particle. The pore formation in recycled powder is attributed to out-diffusion of Mn, S and Si to the outer surface as a result of the incident laser heat during the AM process due to higher electron affinity of such metallic elements to oxygenation. HAXPES analysis shows a higher MnO concentration around the pore area which impedes the in-diffusion of other elements into the bulk and thereby helps to creates a void. The inside wall of the pore area (dendrites), has a higher concentration of Fe and Cr oxide. We believe the higher pore density in recycled powders is due, at least in part to composition redistribution, promoted by laser heat during the AM process. Nanoindentation analyses on both virgin and recycled powder particles shows a lower hardness and higher effective modulus in the recycled powder particles attributed to the higher porosity in recycled powders.

Keywords: additive manufacturing, recycling, pore formation, tomography, 3D printing.

1. INTRODUCTION

The extend and methods of degradation of metal powders that have been processed through PBF are poorly understood. Due to the requirement for high and controlled levels of quality control in parts produced, such degradation can for some applications hinders the ability to recycle the powder. Ideally these would be recycled indefinitely, however, morphological and compositional changes to the powder limit the number of times a powder can be recycled. Degradation of the powder feedstock manifests itself

as a reduction in the mechanical properties of components built using this powder. Hence, a technique is required which allows us to appraise the quality of the powder throughout its life.

Recently, producing parts from recycled metallic powders within the additive manufacturing (AM) process has become an attractive topic for the R&D sector [1, 2]. Reusing the non-solidified metallic powders promotes resource sustainability and resource-efficiency [3]. Several research groups have reported different recycling strategies to reuse the powders for five to more than 30 times [4, 5]. However, they all agree that after a certain number of recycling steps, the mechanical quality of the printed part or the metallurgy of the powder itself becomes a concern. These concerns centre on the increased degree of oxidation on the surface of recycled powder, changes in the particle size distribution (PSD), and porosity formation in the powder [6]. Variations in the chemical composition throughout the particle can also lead to critical variations in the composition of parts fabricated during the manufacturing process. Despite great developments in metal AM, persistent deficiencies and challenges exist in preventing porosity formation, excess surface roughness, and propagation of crack/void which directly impact on the part quality [7]. The internal pores in the particles, which have survived the laser heat and been retained in the melt pool, could also create porosity within the parts. In fact, both virgin and recycled powders contain a range of porosity in many particles. Therefore, further research is required to improve the powder manufacturing and AM dynamics e.g. by improving the gas atomization process or preventing out gassing of the melt pool [8, 9].

We have previously reported a surface composition analysis of both virgin and recycled powders [10] and here we focus on understanding the pore formation and distribution mechanism as well as the pore nature in recycled metallic powders. Porosity may occur in recycled powders for several reasons [11]. Terrassa et al. have observed spherical internal pores in both virgin and recycled stainless steel 316L powder particles using metallographic SEM analysis and attributed these to the atomization process or the laser generated heat during the AM process [12]. They reported that larger pores will form with increasing re-use cycles, suggesting that this is due to incomplete melting, increased agglomeration and more gas inclusion over time. Pores in produced parts can also form due to lack of fusion, called internal voids. This type of pore forms due to partially melted or isolated un-melted particles [13]. Observing pores in the virgin powder suggests an improvement is required in the powder manufacturing process. However, preventing pore formation in the recycled powder requires optimizing the manufacturing conditions to control the powder's dynamic morphology (metallic element distribution) under laser heat and argon flow in the chamber (gas bubble related porosity). X-ray Micro computed tomography is a very reliable measurement technique. Several authors have previously discussed its importance in dimensional metrology for measurement of various micro-features [14]. Heiden et al. have measured the size, distribution, and morphology of the internal porosity in recycled powder particles (316L) using X-ray micro-computed tomography (XCT) [15]. They reported noticeable signs of porosity in both virgin and recycled particles with a slight decrease in pore size and surface/volume of the pores in recycled powder. They attributed this difference to pore collapse with thermal treatment during the laser process or the consumption of porous particles during the process. Pycnometery analysis also confirmed that the pores were breaking up into smaller pores during the AM process leading to a wider pore size distribution for the recycled powder. There are inconsistent reports in the literature on pore size distribution and formation in recycled powders which necessitates further researcher of this phenomenon [16].

The area used by powder bed can also be considered in evaluating the extent of the effect of the manufacturing process on recycled powders. When more area of the powder bed is used and is covered by the powder, then lesser number of particles are affected and most of them are used in the process. Also, the recycled powders will have more homogenous surface and bulk properties since there is not much area for the affected particles to skip from solidification and thus the ejected particles will mostly see a similar impact from the laser heat or from the printing process [8,9]. By applying this concept to several available 3D-printing machines and recording the powder bed area under print, we can have a better idea on how the recycled powders could differ from the virgin powders.

Here, the focus is on pore analysis in both virgin and recycled of 316L powder. The particle and pore size distribution were measured using 3D imaging XCT. The surface and bulk chemical composition were analyzed by synchrotron XPS surface and EDX respectively. The hardness and effective modulus of the powder particles were measured with nanoindentation to analyze the impact of porosity on the particles' mechanical properties. 3D tomography is a capable non-destructive technique as it can image the pores inside the particles even though they may look perfectly solid under the SEM and have a clean surface. The pore density and pore nature in the recycled and virgin powders was examined and the possible reasons of a higher pore density and broader size distribution in recycled powders is discussed. Elemental distribution in the interior side and outside the pores was measured which confirmed the presence of more metallic oxides in the particle pore. Finally, the mechanical properties of the porous areas on the recycled powder were measured to correlate with the microstructure and chemical composition analysis. The dynamic laser melting process in the AM machine and the heat imparted during the AM process can explain the pore formation in the powder particles and the re-distribution (in/out diffusion) of elements resulting in pore formation. Reducing the porosity of the part results in greater part density which would enable AM parts to be produced with higher mechanical properties.

Based on observations from the literature it is therefore necessary to devise a standardized approach for creating recycled powder and evaluating its suitability. In this work, a methodology is proposed alongside a systematic proposal for the use of characterization techniques which are commonly available. Data processing tools were applied in order to ensure that these return communicable data.

2. Materials and Characterization Methods

The commercial gas-atomized powders of stainless steel alloy 316L powder were provided by Castolin Eutectic Ltd. The chemical composition of the powder is as given in Ref. [10]. The average particle size after sieving was 20-35 μm with some finer particles present. AM parts were manufactured using an EOSINT M280 SLM 3D printer at SEAM center in Waterford Institute of Technology (Ireland) and the recycled powders were sieved to remove bigger particles and the spatters, although some ejecta were still present in sieved powder. The number of 9 test cubes of 5 cm^3 were printed and the recycled powder was sampled for characterization from 10 mm distance between the cubes. The apparent density of the virgin powder was 7.99 g/cm^3 [17]. The recycled powder was sampled over 10 printing cycles. These powders were stored in glass vials and capped to minimize atmospheric exposure. They were subsequently moved to the laboratory for characterization as described below. No further surface treatments were performed on the powders after sampling. In previous work, the authors performed various characterization tests on both virgin and recycled powders and reported the difference in their general morphology, surface structure, bulk composition, size distribution and the microstructure to understand how the chemical composition and mechanical properties of the powders change during the AM process [10]. In our previous analysis, the hardness and effective modulus were measured by nanoindentation at different locations on the powder surface. This was then investigated by AFM measurements to examine the results in relation to pore locations, with different microstructures and chemical compositions. This motivated the focus on pore analysis for both powders to understand the nature of porosity in terms of composition and distribution. The results of XCT, HAXPES, and EDX were correlated to determine if the pore formation (especially the trapped pores) was related to composition changes during the manufacturing process. The nanoindentation measurements were also examined to understand the difference between the mechanical properties of both types of particles, virgin and recycled.

2.1. X-ray Computed Tomography (XCT)

X-ray computed tomography (XCT) measurements were performed with a Xradia 500 Versa X-ray microscope (XRM) at the University of Nottingham (UK) with 80 KV and 7 W accelerating voltage [18]. The powders were kept in a polycarbonate tube of 5 mm diameter and placed at 27 mm distance from the X-ray source and 11 mm distance from a 1024x1024 3-axis CCD detector. The pixel size was set at 2 μm, taking about 2.30 hours to complete the 3D scan of the rotating sample around its z-axis in 1600

steps for 0.2 degrees and 6 seconds exposure time. About 1350 particles were measured for each powder sample.

2.2. Synchrotron Hard X-ray Photoemission Spectroscopy (HAXPES)

Synchrotron XPS measurements were performed to analyze the chemical composition (to a depth of approximately 20-30 nm) of the virgin and recycled powders. Hard X-Ray Photoelectron Spectroscopy (HAXPES) measurements were conducted at SOLEIL Synchrotron in France on the Galaxies Beamline [10, 19, 20]. Spectra were acquired at pressures of 10^{-9} mbar with photon beam energies of 10k eV, which allows probing the deep core level of all elements as well as the acquisition of more bulk sensitive spectra using a Si (333) monochromator. Both virgin and recycled powders were measured under these conditions. No chemical treatments were conducted on the particles prior to XPS scans in order to reduce the surface contamination. Powder particles were deposited on an adhesive carbon pad mounted on a 1 cm^2 diameter steel circular stub. The acquired XPS peaks were curve-fitted to their relevant chemical species using CASAxps [21] and AAnalyser [22], using literature values and the NIST X-ray Photoelectron Spectroscopy Database [23].

2.3. Energy Dispersive X-ray Spectroscopy (EDX)

The chemical composition on both type of powder particles was measured especially on open pore areas scanned with an EDX spectrometer of Hitachi S5500 Field Emission SEM system. The particles were imaged at 20 nm scale (15-20 kV). High-resolution images were recorded on the surface and beneath by secondary electron scattering to reveal the chemical composition and distribution.

2.4. Nanoindentation measurements

Nanoindentation hardness tests were performed on both powders using a Bruker HYSITRON TI Premier. For this experiment, cold mounting of the powder particles was performed using two round moulds silicon rubbers. MetPrep Tri Hard solution and powder were used as the based materials and the particles were polished using Metkon Forcipol polisher and using Diamond Suspension of 6 microns, then 1 micron, and then using Silicon Colloida Silica of 0.06 micron. The optical microscope was used to examine the polished surface of the particles at every stage and to confirm where the indents were applied on the particles.

3. Results and Discussion

The characterization results on both virgin and recycled powders were analyzed in search of a correlation between the pore's bulk/surface chemical composition and microstructure acquired from different characterization techniques.

3.1. X-ray Tomography analysis

Over 900 XCT image slices were recorded for each specimen and reconstructed in 3D format using Aviso Software [24] available for use with the XCT machine. Figure 1 presents the 3D rendered image of the virgin powders. The same 3D image was reconstructed for the recycled powder. Cubic regions of interest were selected to categorize the particles in three different sizes and displayed them in different colors. The green, blue and red particles size range were of <20 μm, 20-40 μm and >60 μm, respectively as shown in Fig. 1. The image processing procedure available in the software provides a method to extract the particle and pore size distribution of the specimens from the XCT images. Fig. 1 shows the PSD and volume histogram of the virgin and recycled powders which do not show much difference but a slight overlap of the sizes which means the AM process did not change the particles size significantly. This is in agreement with literature reports on this [25, 26]. The volume of the particles from the 3D reconstructed cube did not show much difference between the two powders. There were more smaller particles in the recycled powder compared to its virgin counterpart probably due to the blowing of smaller particles away from the melt pool during processing, as for this a lower level of kinetic energy would be required [27].

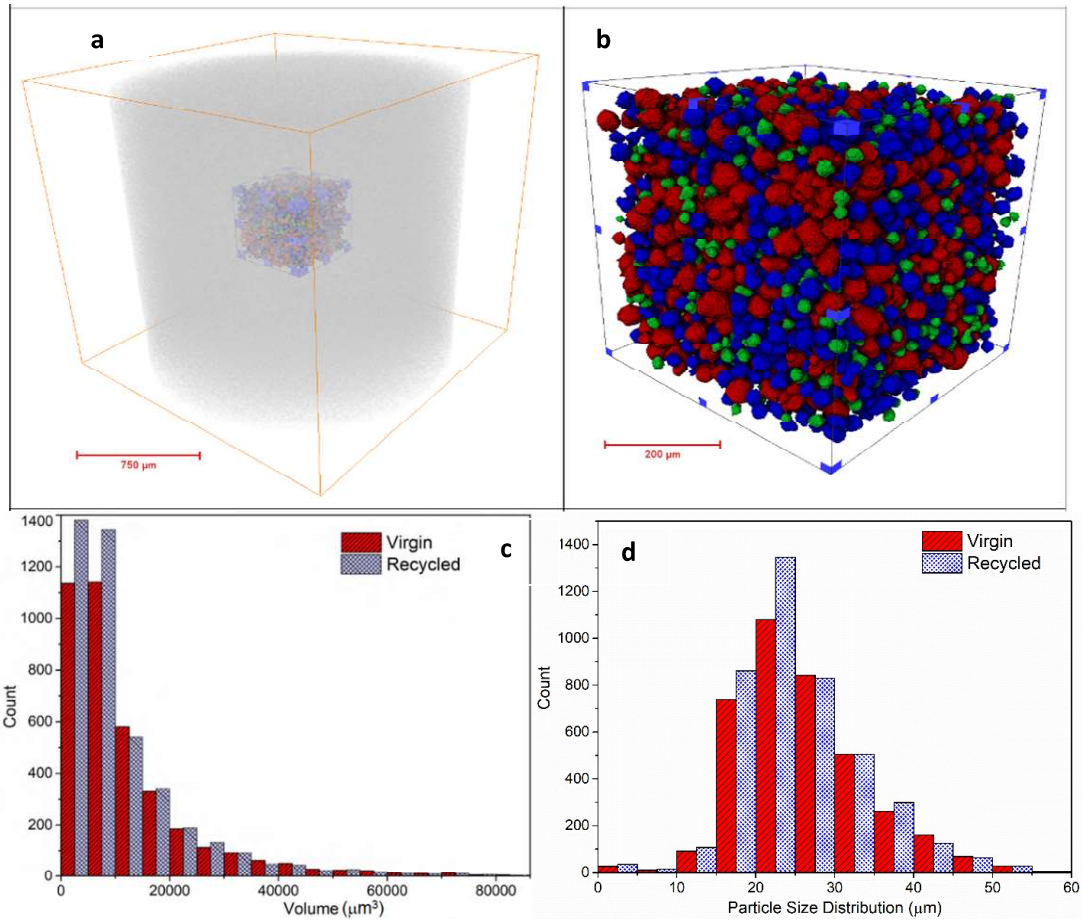

Figure 1. (a) 3D reconstructed representation of XCT images, (b) size distribution of particles in 3 colors, (c) volume histogram, and (d) particle size distribution extracted from XCT images for both the virgin and recycled powders.

Apart from the particle size distribution analysis, extensive testing was carried out using a variety of image processing methods for quantitative pore analysis of the powders [28, 29, 30]. Most literature reports on pore evaluation in manufactured *parts* (and not powders) using the XCT technique [18]. The pore formation in recycled powders from the AM process has been rarely reported in the literature. Such investigations promote an understanding of pore formation dynamics and may suggest possible preventive optimization actions. In fact, XCT is a reliable and accurate technique for this purpose as a non-destructive method and enables the pore shape, position and size distribution analysis [28,31]. 3D imaging of the pores (especially the trapped pores) is preferred over crystallography cross-section analysis of pores because 3D imaging is fast in scan time, does not require any pre-treatment, i.e. polishing and grinding, and is able to scan the whole specimen without requiring manual interference with its structure. To extract the pore size and distribution, over 900 slices (cross-sectional images) of each powder sample were stacked to form the 3D images. Fig. 2 represents the image processing steps that were applied such as threshold adjustment (gray scale threshold), colored classifying, edge cutting, disconnecting the powders and some other manual image processing [18, 28, 29].

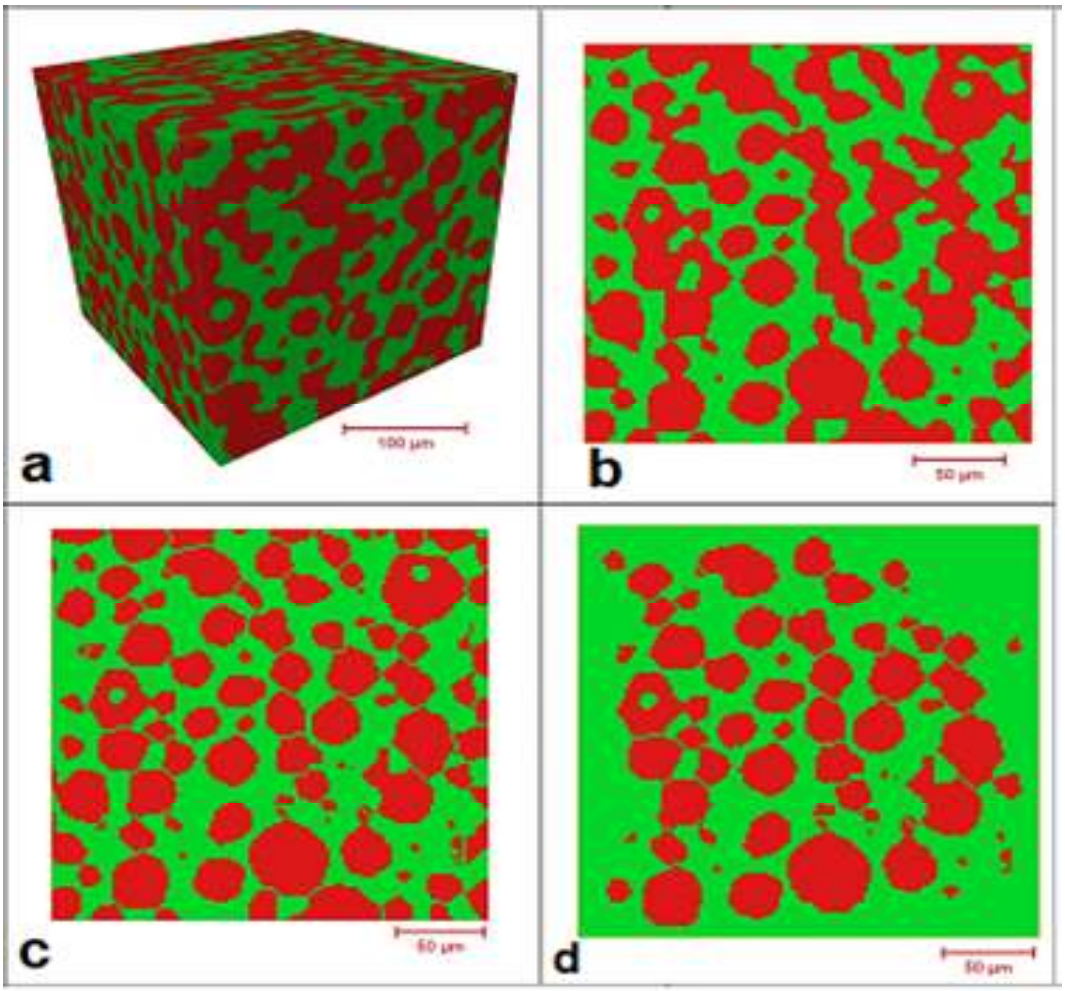

Figure 2 Image processing analysis to extract the pore size distribution in powder samples: (a) 3D reconstruction and color inversion of the pores and gaps, (b) 2D representation of a single slice, (c) isolating of the bonded particles, and (d) removal of the margins.

Fig. 3 (a) presents one slice of a set of images taken from the recycled powder. Trapped pores and open dendrites are visible (shown in red circles). The 3D distribution of pores and the pore size distribution extracted from the image analysis are also shown in Fig. 3 (c) plotted in cumulative frequency mode and d) in chart mode. Fig 3c shows the cumulative frequency distribution for the pores between 5 - 60 μm diameter of both powders. In the virgin powder specimen, pores of 5 μm size contributes to 16.28% of the entire pore population. An increase of 6% is observed in recycling powder. For pore population between 5-10 μm, the virgin powder shows 8% greater pores compared to recycled which can be assigned to thermal impact during the AM process. Also micro-pores (~ 5 microns) develop in recycled powder. Similarly, for the pore population between 5-15 μm, the recycled powder shows 7.74% increase compared to virgin powder. It is thus evident, that new pores of the order 10 to 15 μm develops in recycled powder as expected. Nevertheless, beyond 20 microns, both curves are flattening out, which means that there is no significant difference in the new pores above 20 microns. Overall, the fact that the cumulative frequency curve for the recycled powder is always above the virgin powder specimen, confirms the new pores generation in the recycled powder. The recycled powder has smaller pores than the virgin counterpart but in a broader range. Maskery et al. attributed this to growth of smaller pores due to the decreased cooling rate of the melting pool at the edges [18]. Some literature also reported minor or no change in pore size in the recycled powders [32, 33, 34]. Barnhart reported a significant change in both size (26 μm to 34 μm) and shape of the recycled powders changing from mostly spherical to having

more dendrites open pores [35]. Looking at several single slices in the image set shows a noticeable number of trapped pores in both powders which could not be detected by the other techniques (i.e. SEM or light optical metallography). Table 1 summarizes the morphological properties extracted from XCT analysis. The average size (diameter), average surface area and volume of both powders and pores for virgin and recycled samples were extracted. The data shows that the pore size decreased slightly. This is in agreement with the numbers reported by Heiden et al. where average diameter of 7 μm and 4.4 μm for pores in virgin and recycled powders, were respectively reported [15].

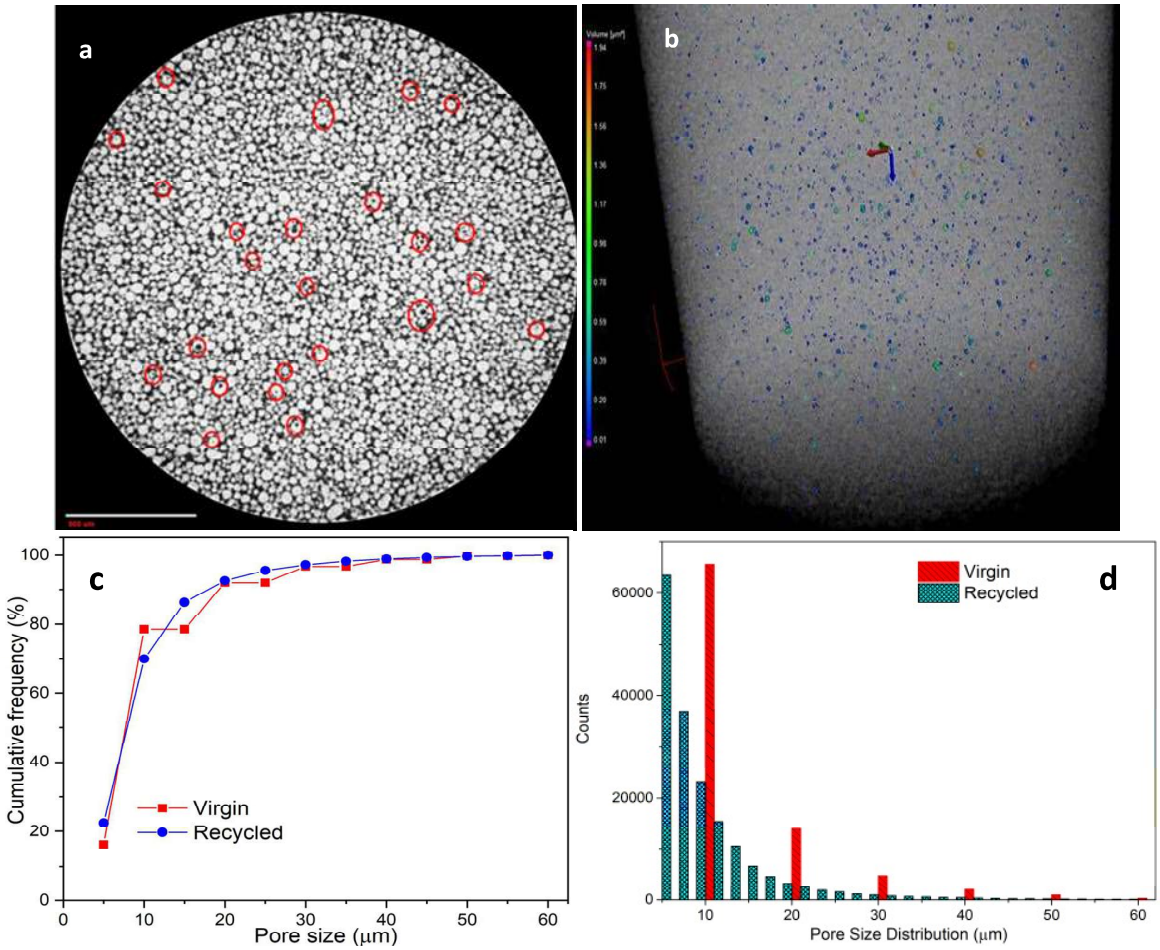

Figure 3. (a) One slice of the XCT images taken from recycled powders with pores of several particles indicated with red circles, (b) pore identification in the 3D reconstructed image, and the pore size distribution of both powders measured from the whole 3D rendered image plotted in c) Cumulative Frequency mode and d) chart patterns.

A negligible average particle size difference for recycled powders (25 μm) versus the virgin powder (26 μm) was recorded which is in contrast to Heiden et al. as they reported a slightly larger average particle size for reused powder (18.5 μm) compared to virgin powder (15.5 μm) [15]. Conversely, Galicki et al. reported a more irregular shape, slight decrease in particle size but a broader size distribution after 30 recycling steps [27]. They also reported a smaller internal pore volume and surface area for the recycled powders and attributed that to pore collapse under application of the laser heat. Nevertheless, our finding is in agreement with most literature reporting a finer size for recycled powders [36, 20, 37, 38]. A smaller average surface area and volume of pores in recycled powder could be as a result of the influence of the laser heat, which breaks the pores into smaller inclusions and fosters their consumption during the laser processing. Terressa et. al [12] measured larger pores in recycled powders assigning this to melting and agglomeration. Simonelli et al. reported a minor or insignificant change in the porosity from metallography

measurement of the both powders [simonelli]. This measurement result is in agreement with the results found in this work where negligible change in pore size was also recorded.

Table 1 Average particle and pore diameter, surface area and volume, from XCT measurements.

Powder	Average Diameter (μm)	Average Surface Area (μm^2)	Average Volume (μm^3)
Virgin	26(±8)	2350(±1500)	12200(±12520)
Recycled	25(±7)	2223(±1430)	11240(±11650)
Virgin pores	10(±8)	521(±1000)	2085(±7778)
Recycled pores	9(±7)	418(±900)	1633(±6846)

3.2. EDX composition analysis

EDX analysis on electron backscatter on the pore area was conducted and the results are presented in Fig. 4. Both powders show a similar EDX spectrum with comparable peaks for C, O, Si, S, Cr, Mn, Fe and Ni which is in agreement with our previous report on the concentration of such elements in these powders [10]. It is possible to obtain the composition from open pore areas and not from trapped pores. Open pores are dendrites or pores forming at edges and the trapped pores are vacant inside the particle away from the edges. The EDX map created for an open-pore (a porous particle halved from center) in a recycled particle is displayed in Fig. 5 with the concentration of carbon and oxygen across the particle. There is a uniform distribution of these two elements across the particle, which is not surprising. Fig. 6 shows the EDX composition map of other elements inside and around the pore area. Interestingly the Fe, Cr and Ni are more concentrated inside the pore area whereas Si, S, and Mn are mostly concentrated outside and around the pore area. This observation could reveal a diffusion process of metallic elements during the AM process. Barnhart reported a high concentration of metal oxides of Fe and Cr with a thicker Si oxide layer (5-7 times thicker) on the surface of recycled powder [35]. Note that Cr and Si have higher O affinity, according to Ellingham Diagrams, and form a thick oxide in presence of oxygen. In contrast, Ni and Mn have low O affinity and are less subject to oxide formation. However, Mn has a high tendency to diffuse to the surface during the AM process. Therefore, a lower Fe and Ni concentration but a higher concentration of Mn-oxide and Si-oxide has been detected on the surface of the recycled 316L powders. Mn and Si surface enrichment is assigned to their high volatility, high diffusion rate. This reveals the diffusion of metallic elements of oxide formation in or outside the pore or on the particle surface as a guide to optimize our laser processing. However, in agreement with the EDX measurement on recycled particles, the Synchrotron HAXPES measurements, as presented in Fig. 7, show that only Cr oxides form in the bulk part.

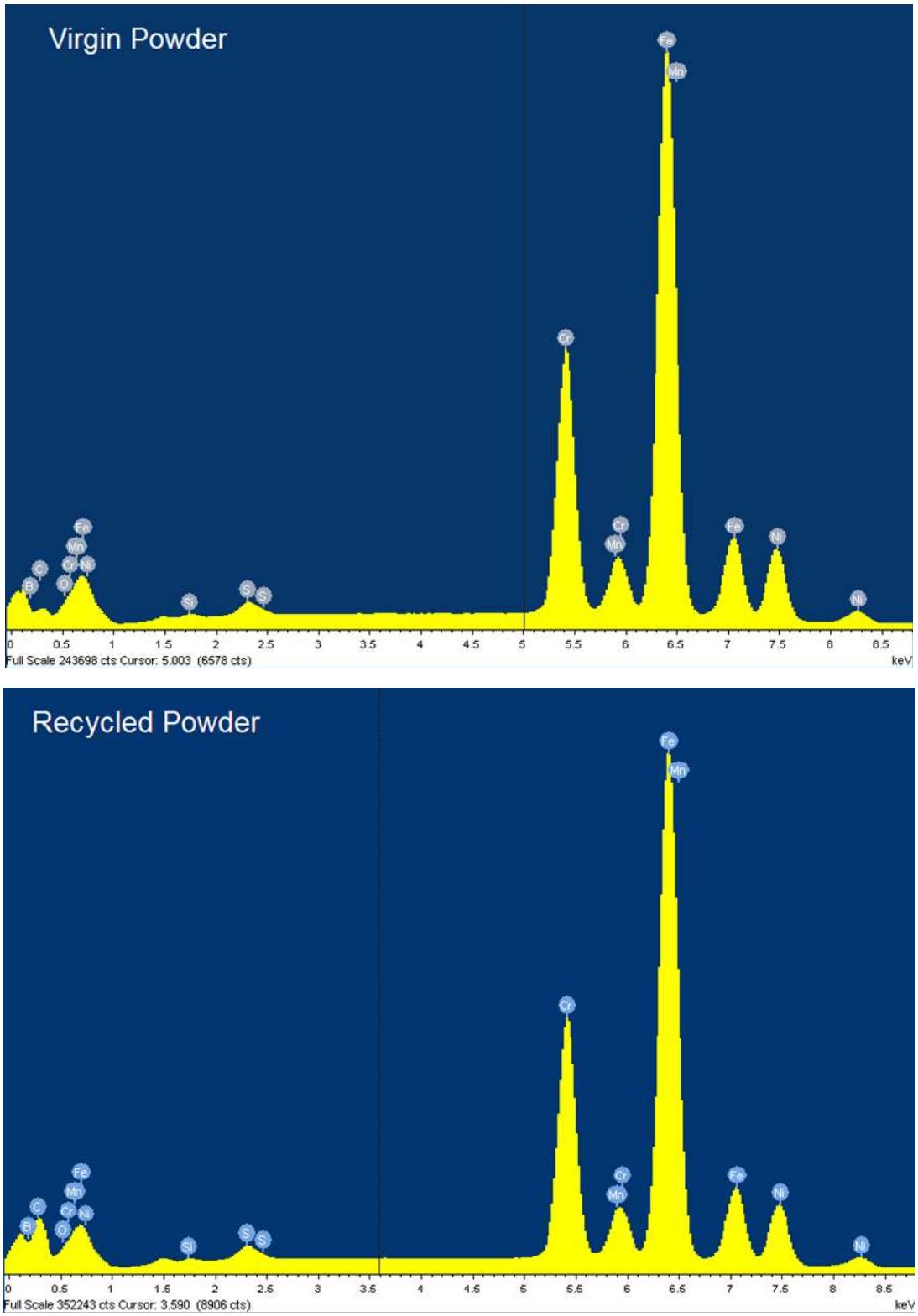

Figure 4 EDX spectrum of each virgin and recycled powder. Most peaks overlap well for both powder samples. The highest peaks belong to Fe, Cr, and Ni and there are S, Si and Mn with weaker peaks. C and O are also present as expected.

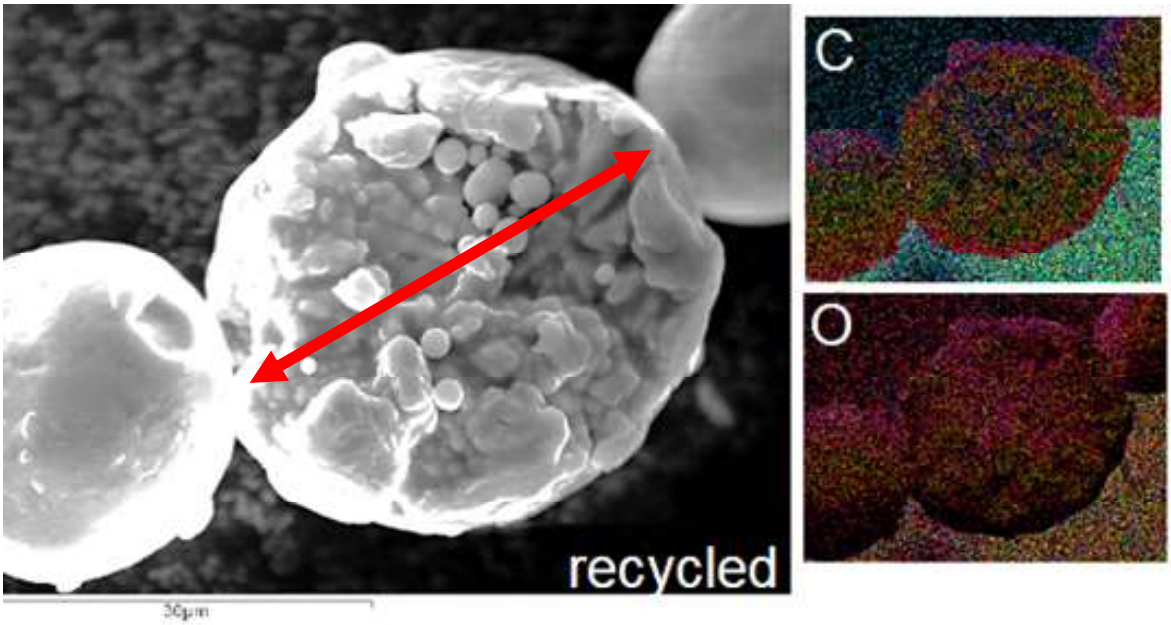

Figure 5 Open pore in a recycled particle images with EDX. The carbon and oxygen composition map across the pore shows a uniform distribution of the two elements. The red arrow shows the EDX line scan direction.

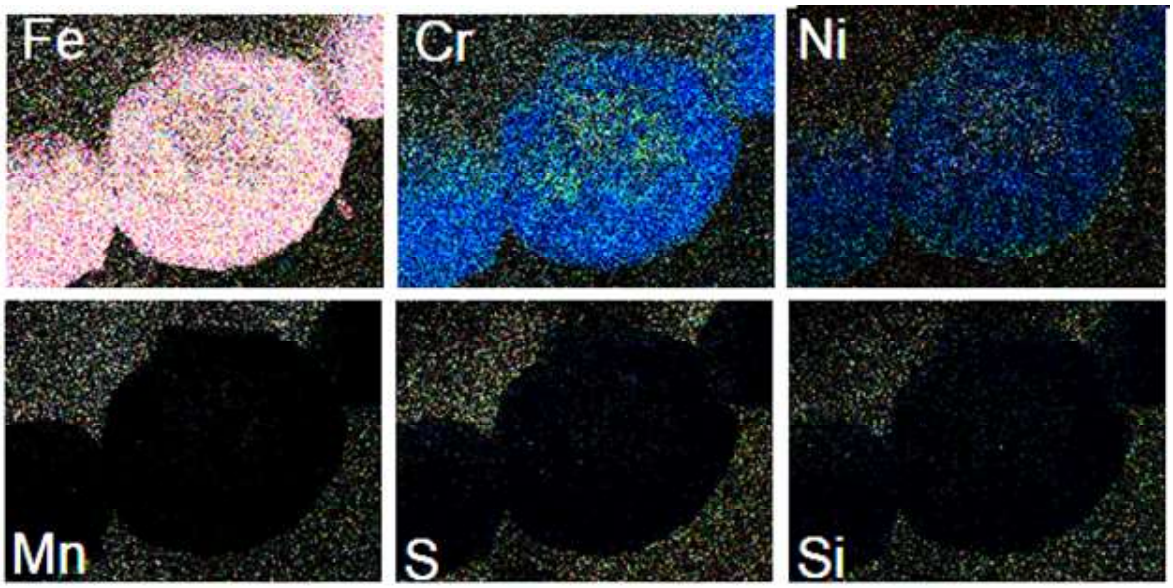

Figure 6, EDX compositional map of various elements inside and around the open pore in a recycled particle. Three elements of Fe, Cr, and Ni (top) are more concentrated inside the pore, and the other elements Mn, Si and S are more distributed outside and around the pore area.

3.3. Synchrotron HAXPES composition analysis

HAXPES can be used to reveal the chemical composition through the photoemission of core level electrons from the particles of the stainless steel [39] to a depth of about 20-30 nm. Therefore, it can confirm the presence of elements across the pore area trapped inside the particles. To the best of our knowledge, such measurements have not been reported for recycled powders within the AM process to date. Figure 7 shows the HAXPES measurements on the recycled and virgin powders by element

composition analysis.. Different metallic components show peaks at different binding energies, which represent the orbitals from which the electrons have been emitted. The elemental concentration on the recycled powders were previously measured and showed that the C and O concentration increases more than any other element on the surface of recycled powder compared to virgin powders [10, 40]. Here, the peaks from elements observed in EDX map are reported in order to make a correlation between the two experiments. Figs. 7 shows the HAXPES 1s peaks for Fe, Cr, Ni, Mn, S, and Si. The recycled powder has a large Fe 1s peak, indicating a higher surface concentration of Fe after recycling. There is almost a same metallic Cr concentration but a higher Cr-oxide on recycled powder in correlation with the EDX data. The metallic Mn signal increases slightly indicating a higher concentration of metallic Mn at the surface in recycled powders. The Si and S peaks are largely unchanged and Ni signal reduces significantly indicating a diffusion of nickel away from the surface during the laser melting process. The metal oxides presented in the results such as FeO, Fe_2O_3, CrO, Cr_2O_3 and NiO were only observed in recycled powder, or had a higher concentration in recycled powder. In general, the increase in oxidation happens by heating the sample e.g. by laser heat during AM the process. Terressa et al. also reported Mn_2O_3, Cr_2O_3 and Fe_2O_3 in the recycled powder [12]. They related this to imperfect vacuum cleaning of the SLM machine, impurities with oxidation present on the surface, heat and the oxygen released from the inclusion sites inside the melted particles. The higher concentration of Fe, Cr and Ni oxides are explained at the surface together with the reduction in Ni in the near surface region of the recycled powder by a dynamic diffusion of other elements to the outer surface under laser heat process. In fact, Cr_2O_3 is the most stable oxide of the above mentioned metal oxides and will form first [19]. In 1997, Kimura et al. have shown that heating Mg soluted in aluminum alloy powders moves out from the inner region to the outer surface at higher temperature by breaking the surface oxide films and forming metallic aluminum on the particles' surface [41]. The oxidation rate also has an effect on the diffusion rate of the metals because formation of a thicker oxide layer will reduce or block the in-diffusion of the elements which can leave a void inside the particles. This may be more probable in the recycled powders as they experience continuous laser heat during the SLM process. For example, when Mn diffuses out to the surface of the particle, the Fe and Cr remain inside. Then S or Si cover the particle surface and block the oxygen or Mn to return into interior part of the particle thus leaving a pore or void area inside. This definition is also in agreement with EDX results as the Mn, Si and S are mostly outside the pore area while Fe, Cr, and Ni are also inside the pore area. An alternative conventional explanation is that the oxygen inclusion in the bulk of the particle creates the pores mostly observed in printed parts rather than in powder particles [18].

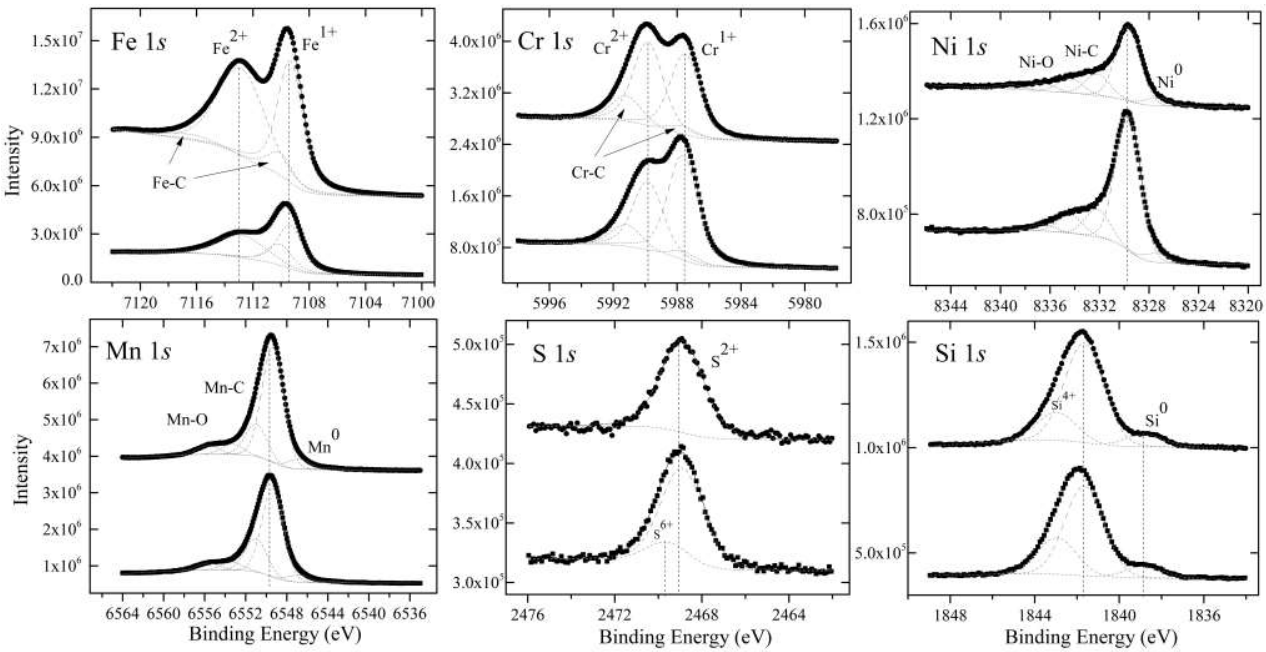

Figure 7. HAXPES measurements on the recycled and virgin powders by element composition analysis at 10kV beam energy.

3.4. Nanoindentation measurements

It is known that porosity is detrimental to the mechanical properties of the powder and parts, and results in lower strength and fatigue for the porous materials [19]. Pores can also propagate to cause cracks and further stress concentration. To understand the mechanical properties of the powders, nanoindentation was performed on both virgin and recycled powder samples [10]. Several nanoindentation tests were applied at different locations on randomly selected particles of both powders (F=250 μN for 5-10 seconds). A lower average hardness was obtained from the recycled powders. Here, further measurements are presented after monitoring the pore areas on the polished surface of the particles under the microscope of the same nanoindentation system. Fig. 8 presents the hardness, and effective modulus measured for different depths on both samples. The recycled particles show lower hardness and higher modulus at different indentation depths. These are assigned to the presence of pores beneath or around the indented areas. However, other factors can also contribute to this. For example, the recycled powder particles may be degraded. The metal oxides, which are more present in the recycled powder, have a higher molecular weight and reduce the mechanical strength of the recycled powders [42]. Terressa et al. reported no statistical relation between the microhardness of the recycled powder and the cycle number [12]. Sartin et al. reported a minor change (0.2%) on tensile strength of the recycled powder and part [26]. Heiden et al. reported a slightly higher roughness on the recycled powders attributed to dendrite exterior on the particle or open pore formation on surface [15].

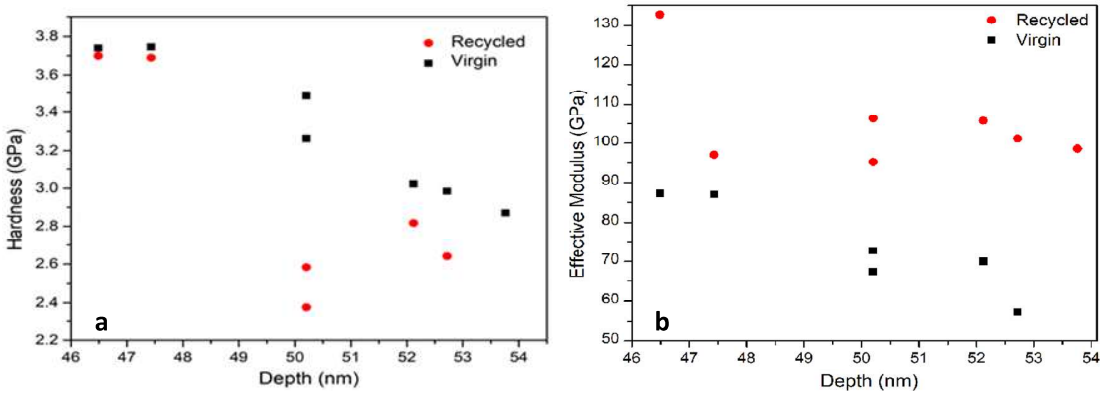

Figure 8 Nanoindentation measurements showing the (a) hardness and (b) effective modulus obtained for both recycled and virgin powder on different indentation on different porous locations of the particles.

4. Pore formation mechanism in recycled powders

The internal pores in recycled powders (not in printed parts) has been less investigated in literature [43]. Most research groups have examined the pore formation in printed parts which could either be manufactured from the recycled powders or a mix of virgin and recycled ones. Nevertheless, the pore formation in recycled powders can shed light on optimizing the PBD process itself or the strategy to reuse the powder in further reusing cycles. Note that pores could be source of oxygen or contamination and can cause pore formation in printed parts with undesired mechanical properties [18]. Saboori et al. measured a lower elongation for the parts made of recycled powders compared to the parts made of virgin powder due to a lower inclusion content and of lower average size of the recycled powders [43]. According to EDX results, the pores contain Cr and Si-oxides due to high oxygen affinity of such elements even at a reduced gas flow rate with minimized oxygen content. The characterization results presented here provides an insight into the pore formation mechanism in recycled powders. Especially, XCT images revealed the porosities with average cross-sectional diameters of 8 μm which is slightly smaller than the pores in virgin powders (10 μm). The pore shape in recycled powder distributions did not change significantly compared to its virgin counterpart. However, some clustered pores were observed even if the virgin powder was sieved. The powder bed geometry of our EOS printer is 250 mm x 250 mm x 250 mm. The number of 9 test cubes of 10 mm^3 were printed. The rest of the powder bed was used to print number of tensile test bars. The recycled powder was sampled for characterization from 10 mm distance between the cubes. In total, only 25% of the powder bed was used for printing the cubes and bars and the recycled powders were sampled from 120 mm^2 area remained between the cubes (from one of the 10 mm channels between the cubes). The area of 250 mm^2 of the powder bed is occupied with test cubes and the distanced between them. The periphery area around the cubes is also covered by the powders. The percentage of the total area used by the 3D printer is calculated by,

Used are of powder bed for printing = *(total cubes surface area) / total area of the powder bed*

It is believed that the powders remained between the cubes are the most impacted powders although it can still be mixed with untouched particles. Therefore, the small variation in size of the virgin and recycled powder can be understood as the powder bed size is large compared to the area used to print the test cubes. A smaller powder bed may increase the number of spatters or the population of the affected particles in recycled powder resulted in a different pore size distribution [44]. Martin et al. have attributed the pores formation to melt pool dynamic due to rapid formation when excess energy is imparted by laser to melt pool [7]. Thus they suggested modulating the laser power to compensate for melt pool overheating and pore formation.

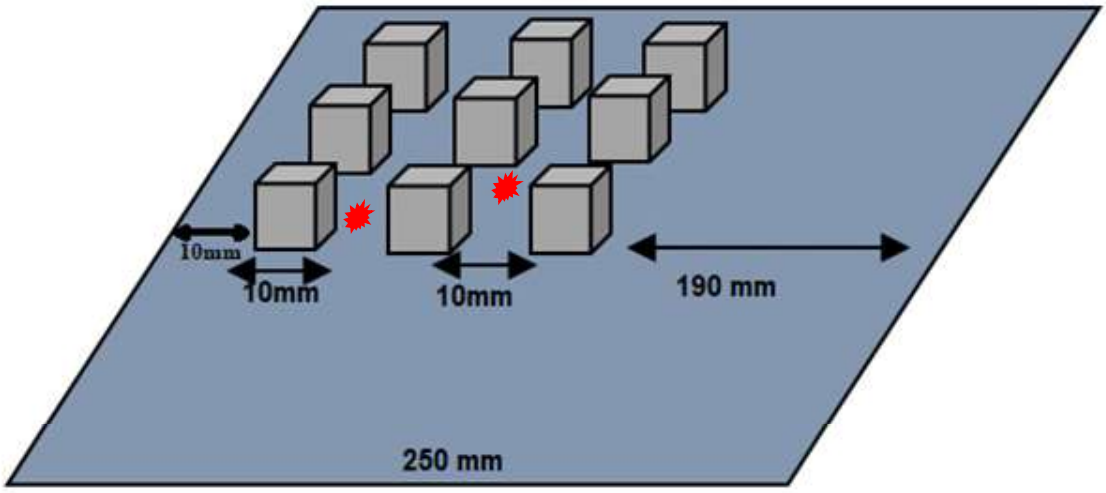

Figure 9 the powder bed and the printed test cubes with the given dimensions. The recycled powders were sampled from 10 mm distance between the cubes shown by the red indicators after over 10 times recycling.

The XCT measurements show a slightly increased number and volume of the recycled powders. This is in agreement with the report of Gasper et al. showing that the particles of up to six times larger can also exist in recycled powder such as ejected spatters [45]. We have previously shown that although the recycled powder was sieved, the clustered particles and elongated spatters still observed in the recycled powder [10].

5. Conclusion

Pore formation in powders and parts is still a challenging problem in AM processes. The solution to this problem is to provide and use powder feedstock which does not have pores, as much as possible, and to implement a control strategy which mitigates pore formation during the process. A better understanding on pore formation and nature will help to develop strategies to prevent them for occurring. The pore nature and formation were investigated in powder particles of recycled and virgin 316L powders within an additive manufacturing SLM process. The recycled powders show slightly more porosity inside the powder particles as confirmed with X-ray computing tomography. The pores have more iron and chromium inside whereas the Mn, Ni, and Si were mostly distributed outside and on periphery of the pore areas. This understanding was confirmed with synchrotron XPS analysis where the higher concentration of Fe and Cr from recycled powder were confirmed. Nanoindentation was performed to measure the mechanical properties of the particle and the recycled powders have shown lower hardness and higher modulus at different indentation depths, which would be expected to be due to the higher level of porosity in these powder particles. The pore formation in recycled powders is more probable when the powder bed is more occupied by the printing parts since the number of affected particles increases if more area of the powder bed is used for printing. Therefore, apart from the chemical reorganization of the elements during the printing process, the used powder bed area can also give us a useful idea on the extent of the impacted powders. Therefore, we suggest to record the powder bed area used for printing during the process for every 3D-printing machine.

6. Acknowledgment

This research is supported by a research grant from Science Foundation Ireland (SFI) under Grant Number 16/RC/3872 and is co-funded under the European Regional Development Fund. We acknowledge Dr. B. O'Connell for his valuable assistance in running the characterization and measurements. N.E. Gorji Acknowledges the New Foundation Award (No. P60687) received from Irish Research Council (2019) and also the ECIU Research Mobility (No. P60617) grant (2018). The authors

would like to thank SOLEIL Synchrotron for using their HAXPES measurement facilities as well as the support given by the beamline scientists (SOLEIL proposal No. 20180106).

References

[1] R. Galantea, C.Pina, A. Serro, ''Additive manufacturing of ceramics for dental applications: A review'', *Dental Materials*, 35 (2019) 825-846. https://doi.org/10.1016/j.dental.2019.02.026.

[2] A. Madrida, S. Vrech, M. Sanchez, A. Rodriguez, ''Advances in additive manufacturing for bone tissue engineering scaffolds'', *Materials Science & Engineering C*, 100 (2019) 631–644. https://doi.org/10.1016/j.msec.2019.03.037.

[3] Nascimento, D.L.M., Alencastro, V., Quelhas, O.L.G., (...), Lona, L.R., Tortorella, G., ''Exploring Industry 4.0 technologies to enable circular economy practices in a manufacturing context: A business model proposal'', *Journal of Manufacturing Technology Management*, 30(3), pp. 607-627. https://doi.org.10.1108/JMTM-03-2018-0071.

[4] H.P. Tang, M. Qian, N. Liu, X. Z. Zhang, G.Y. Yang, J. Wang, '' Effect of Powder Reuse Times on Additive Manufacturing of Ti-6Al-4V by Selective Electron Beam Melting'', *JOM*, 67:3 (2015) 555-564. https://doi.org/10.1007/s11837-015-1300-4.

[5] G. Jacob, Ch. Brown, A. Donmez, S. Watson, J. Slotwinski, ''Effects of powder recycling on stainless steel powder and built material properties in metal powder bed fusion processes'', NIST Advanced Manufacturing Series 100-6, (2016), https://doi.org/10.6028/NIST.AMS.100-6.

[6] T. Debroy, L. Wei, J. Zuback, T. Mukherjee, J. Elmer, J. Milewski, W. Zhang, ''Additive manufacturing of metallic components - Process, structure and properties. *Progress in Materials Science*, *92* (2018) 112-224. https://doi.org/10.1016/j.pmatsci.2017.10.00.

[7] A. Martin, N. Calta, S. Khairallah, J. Wang ,P. Depond, A. Fong, V. Thampy, G. Guss, A. Kiss, K. Stone, Ch. Tassone, J. N. Weker, M. Toney, T. Buuren, M. Matthews, ''Dynamics of pore formation during laser powder bed fusion additive manufacturing*'', Nature Communications,* (2019) 10:1987, https://doi.org/10.1038/s41467-019-10009-2

[8] L. E. Murr, ''A Metallographic Review of 3D Printing/Additive Manufacturing of Metal and Alloy Products and Components'', *Metallography, Microstructure, and Analysis,* 7 (2018) 103-132. https://doi.org/10.1007/s13632-018-0433-6.

[9] M. L. Günther, C. Gebbe, T. Kamps, C. Seidel, G. Reinhart, '' Powder recycling in laser beam melting: strategies, consumption modeling and influence on resource efficiency'', *Production Engineering,* 12:3 (2018) 377-389. https://doi.org/10.1007/s11740-018-0790-7.

[10] N.E. Gorji, R. O'Connor, A. Mussatto, M. Snelgrove, P. G. Mani González, D. Brabazon, ''Recyclability of Stainless Steel (316L) powder within the additive manufacturing process'', *Materialia*. Materialia 8 (2019) 100489. https://doi.org/10.1016/j.mtla.2019.100489.

[11] J. C. Chekotu, R. Groarke, K. O'Toole, D. Brabazon, '' Advances in Selective Laser Melting of Nitinol ShapeMemory Alloy Part Production'', Materials, 2019, 12, 809; https://doi:10.3390/ma12050809.

[12] K. Terrassa, J. Haley, B. MacDonald, J. Schoenung, ''Reuse of powder feedstock for directed energy deposition'', *Powder Technology,* 338 (2018) 819-829. https://doi.org/10.1016/j.powtec.2018.07.065.

[13] K. Darvish, Z. Chen, T. Pasang, ''Reducing lack of fusion during selective laser melting of CoCrMo alloy: effect of laser power on geometrical features of tracks'', *Mater Des*, 112 (2016) 357-66. https://doi.org/10.1016/j.pmatsci.2017.10.001.

[14] P. Saxena, G. Bissacco, A. Stolfi, L. D. Chiffre, Characterizing Green Fiber Bottle prototypes using Computed Tomography, in: *7th Conference on Industrial Computed Tomography*, (iCT 2017), Leuven, Belgium, 2017.

[15] M. Heiden, L. Deibler, J. Rodelas, J. Koepke, D. Tung, D. Saiz, B. Jared, ''Evolution of 316L stainless steel feedstock due to laser powder bed fusion process'', *Additive Manufacturing*, 25 (2019) 84-103. https://doi.org/10.1016/j.addma.2018.10.019.

[16] C. Kelly, N. Evans, C. Irvin, S. Chapmand, K. Galle, D. Safranski, ''The effect of surface topography and porosity on the tensile fatigue of 3D printed Ti-6Al-4V fabricated by selective laser melting'', Materials Science & Engineering C 98 (2019) 726–736, https://doi.org/10.1016/j.msec.2019.01.024.

[17] É. McCarthy, R. Groarke, C. Danilenkoff, S. Karam, M. Bastien, A. O'Neill, R. Raghavendra, A. Staub, A.B. Spierings, D. Brabazon, ''Characterization of Selective Laser Melting (SLM) produced parts using a variety of 316L stainless steel powders'', 2019, under review

[18] I. Maskery, N. Aboulkhair, M. Corfield, C. Tuck, A. Clare, R. Leach, ''Quantification and characterisation of porosity in selectively laser melted Al–Si10–Mg using X-ray computed tomography'', Materials Characterization 111 (2016) 193-204. https://doi.org/10.1016/j.matchar.2015.12.001.

[19] C. Leunga, S. Marussi, M. Towrie, J. Garciae, R. Atwood, A. Bodey, J. Jones. Ph. Withers, P. Lee, ''Laser-matter interactions in additive manufacturing of stainless steel SS316L and 13-93 bioactive glass revealed by in situ X-ray imaging'', *Additive Manufacturing,* 24 (2018) 647–657, https://doi.org/10.1016/j.addma.2018.08.025.

[20] Rueff, J.-P.; Ablett, J. M.; Céolin, D.; Prieur, D.; Moreno, T.; Balédent, V.; Lassalle-Kaiser, B.; Rault, J. E.; Simon, M.; Shukla, A. The GALAXIES Beamline at the SOLEIL Synchrotron: Inelastic X-ray Scattering and Photoelectron Spectroscopy in the Hard X-ray Range J. Synchrotron Radiat. 2015, 22, 175– 179.
[21] http://www.casaxps.com/casaxps-training/bgn_course/bg_index.htm
[22] M. Snelgrove, P. Mani-Gonzalez, J. Bogan, R. Lundy, J.P. Reuff, G. Hughes, P. Yadav, E. McGlynn, M. Morris, R. O'Connor, *Journal of Physics D: Applied Physics,* 52:43 (2019) 435301.
[23] https://srdata.nist.gov/xps/
[24] https://www.thermofisher.com/ie/en/home.html
[25] M. Simonelli, C. Tuck, N. T. Aboulkhair, I. Maskery, I. Ashcroft, R. D. Wildman, R. Hague, '' Study on the Laser Spatter and the Oxidation Reactions During Selective Laser Melting of 316L Stainless Steel, Al-Si10-Mg, and Ti-6Al-4V'', *Metal. Mat. Transac.* A, 46A (2015) 3842-3852. https://doi.org/10.1007/s11661-015-2882-8.
[26] B. Sartin, T. Pond, B. Griffith, W. Everhart, L. Elder, E. Wenski, C. Cook, D. Wieliczka, W. King, A. Rubenchik, S. Wu, B. Brown, C. Johnson, and J. Crow, ''316L Powder Reuse for Metal Additive Manufacturing'', *Solid Freeform Fabrication, Proceed.* 28th *Ann. Int.* (2017) 351-365. https://doi.org/10.1016/j.powtec.2018.07.065
[27] D. Galicki, F. List, S. S. Babu, A. Plotkowski, H.M. Meyer, R. seals, C. Hayes, ''Localized Changes of Stainless Steel Powder Characteristics During Selective Laser Melting Additive Manufacturing'', *Metallurgical and Materials Transactions A,* 50A (*2019)* 1582-1606. https://doi.org/10.1007/s11661-018-5072-7.
[28] C. Willson, N. Lu, W. J. Likos, Quantification of Grain, Pore, and Fluid Microstructure of Unsaturated Sand from X-Ray Computed Tomography Images, *Geotechnical Testing Journal*, 35:6 (2012), http://dx.doi:10.1520/GTJ20120075.
[29] J. Liu, Ch. Liu, Y. Bai, P. Rao, Ch. Williams, Zh. Kong, '' Layer-wise Spatial Modeling of Porosity in Additive Manufacturing'', *IISE Transactions*, https://doi.org/10.1080/24725854.2018.1478169.
[30] P. Saxena, G. Bissacco, F. J. Bedka, A. Stolfi, ''Tooling for production of the Green Fiber Bottle'', *Procedia CIRP,* 69 (2018) 348 - 353. https://doi.org/10.1016/j.procir.2017.12.001.
[31] K .Heim, F.Bernier, R.Pelletier, L. P. Lefebvre, ''High resolution pore size analysis in metallic powders by X-ray tomography'', *Case Studies in Nondestructive Testing and Evaluation*, 6 (2016) 45–52. http://dx.doi.org/10.1016/j.csndt.2016.09.002.
[32] P. Nandwana, W. H. Peter, R. R. Dehoff, L. E. Lowe, M. M. Kirka, F. Medina, S. S. Babu, ''Recyclability Study on Inconel 718 and Ti-6Al-4V Powders for Use in Electron Beam Melting'', *Metallurgical and Materials Transactions* B, 47B (2016) 754-762. https://doi.org/10.1007/s11663-015-0477-9.
[33] E. JELIS, M. CLEMENTE, S. KERWIEN, N. M. RAVINDRA, M. R. HESPOS, '' Metallurgical and Mechanical Evaluation of 4340 Steel produced by Direct Metal Laser Sintering'', *JOM*, 67:3 (2015) 582-590. https://doi.org/10.1007/s11837-014-1273-8.
[34] P. D. Nezhadfar, A. Soltani-Tehrani, A. Sterling, N. Tsolas, N. Shamsaei, ''The Effects of Powder Recycling on the Mechanical Properties of Additively Manufactured 17-4 PH Stainless Steel'', *Solid Freeform Fab. Proceed.* 29th *Ann. International,* (2018) 1292-1300.
[35] B. K. Barnhart ''Characterization of powder and the effects of powder reuse in selective laser melting'', *Case Western Reserve University*, PhD thesis. (2017).
[36] B. A. Hann, '' Powder Reuse and Its Effects on Laser Based Powder Fusion Additive Manufactured Alloy'', *SAE International*, 01 2071 (2016) 209-2014. http://doi:10.4271/2016-01-2071.
[37] J. A. Slotwinski, E. J. Garboczi, P. E. Stutzman, C. F. Ferraris, S. S. Watson, M. A. Peltz, '' Characterization of Metal Powders Used for Additive Manufacturing'', *Journal of Research of the National Institute of Standards and Technology,* 119 (2014) 460-494. http://dx.doi.org/10.6028/jres.119.018.
[38] M. Yakout, M. A. Elbestawi, S. C. Veldhuis, ''On the characterization of stainless steel 316L parts produced by selective laser melting'', *Int. J. Adv. Manuf. Technol*. (2018) 95:1953-1974. https://doi.org/10.1007/s00170-017-1303-0.
[39] A. Herrera-Gomez, "Simultaneous data fitting in ARXPS", Internal Report, CINVESTAV-Unidad Queretaro, http://www.qro.cinvestav.mx/~aanalyzer/SimultaneousFitting.pdf.
[40] N.E. Gorji, R. O'Connor, D. Brabazon, '' XPS Analysis of virgin and recycled metallic powders for 3D printing applications", *ModTech International Conference - Modern Technologies in Industrial Engineering*, Iasi, Romania, June 2019.
[41] A. Kimura, M. Shibata, K. Kondoh, Y. Takeda, M. Katayama, T. Kanie, and H. Takada, ''Reduction mechanism of surface oxide in aluminum alloy powders containing magnesium studied by x-ray photoelectron spectroscopy using synchrotron radiation'', Appl. Phys. Lett. 70, 3615 (1997); https://doi.org/10.1063/1.119250
[42] A. Aversa, M. Lorusso, G. Cattano, D. Manfredi, F. Calignano, E. Ambrosio, S. Biamino, P. Fino, M. Lombardi, M. Pavese, ''A study of the microstructure and the mechanical properties of an AleSieNi alloy produced via selective laser melting'', *Journal of Alloys and Compounds* 695 (2017) 1470-1478. http://dx.doi.org/10.1016/j.jallcom.2016.10.285.
[43] A. Saboori, A. Aversa, F. Bosio, E. Bassini, E. Librera, M. D. Chirico, S. Biamino, D. Ugues, P. Fino, M. Lombardi, ''An investigation on the effect of powder recycling on the microstructure and mechanical properties of

AISI 316L produced by Directed Energy Deposition'', *Materials Science & Engineering A,* 766 (2019) 138360. https://doi.org/10.1016/j.msea.2019.138360

[44] W. Niu, C. Bai, G. Qiu, Q. Wang, ''Processing and properties of porous titanium using space holder technique'', *Mater. Sci. Eng. A,* 506 (2009) 148-151. https://doi.org/10.1016/j.msea.2008.11.022

[45] A.N.D. Gasper, B. Szost, X. Wang, D. Johns, S. Sharma, A.T. Clare, I.A. Ashcroft, "Spatter and oxide formation in laser powder bed fusion of Inconel 718", *Additive Manufacturing,* 24 (2018) 446-456. https://doi.org/10.1016/j.addma.2018.09.032